Molecular Dynamics of Ice-Nanotube Formation Inside Carbon Nanotubes

Junichiro Shiomi,[†,‡] Tatsuto Kimura,[§,||] and Shigeo Maruyama*[,†]

Department of Mechanical Engineering, The University of Tokyo, 7-3-1 Hongo, Bunkyo-ku, Tokyo, 113-8656 Japan, and Department of Mechanical Engineering, Kanagawa University, 3-27-1 Kanagawa-ku, Yokohama-shi, Kanagawa, 221-8686 Japan

Received: February 22, 2007; In Final Form: June 3, 2007

The phase transition of a water cluster confined in a flexible single-walled carbon nanotube is investigated using a classical molecular dynamics (MD) method. The formation of ice-nanotube is monitored through the structure factor and potential energies. The transition temperature and its diameter dependence obtained by the simulations agree well with those of previously reported experiments. The transition temperature of the ice-nanotube was shown to take a maximum value of around room temperature with the number of the ring members $n = 5$. Potential energy contribution to the phase change is generally dominated by that of the intrinsic water−water interaction, while that of water−carbon interaction plays a significant role in determining the dependence of transition temperature on the nanotube diameter.

1. Introduction

Investigation of water confined in low dimension holds much importance as it is a key system in bioscience[1] and nanotechnology under aqueous environments. The confinement is expected to alter the phase transition and various transport properties of water from those of bulk water. An ultimate realistic case of such low-dimensional systems is water confined in single-walled carbon nanotubes (SWNTs). An anomalous phase transition of water to ice-nanotube was first predicted by classical molecular dynamics (MD) simulations of water inside a rigid SWNT under high pressure (axial pressure of 50−500 MPa).[2] It was found that the water experiences a first-order phase transition to form an ice-nanotube (I-NT), where the number of members of the circumferential ring (n) was determined by the diameter (d) of the surrounding SWNT. Molecular simulations have been also used to explore detailed structures of the confined water and their energetic properties.[3,4] The existence of ice-nanotubes was first confirmed in experiments using X-ray diffraction analyses.[5,6] Experiments were performed at around the saturated vapor pressure, where condensation of water inside SWNTs occurred around 315−330 K. The experiments delivered a striking feature of the phase change that the ordering transition temperature increases, even to room temperature, as the nanotube diameter; i.e., n of I-NT decreases. This trend is opposite from that of the bulk water in a glass capillary tube[7] and hence indicates a crossover of physics from bulk to atomic scale phenomena on reducing the diameter.[6]

In the current study, we investigate the diameter dependence of the transition temperature of a saturated water cluster locally confined in an SWNT by monitoring instantaneous molecular structures and potential energy. While the transition temperature has been calculated for various nanotube diameters (or n) by MD simulations[2] and grand canonical Monte Carlo simulations,[4] the current work is first to provide the direct comparison with the experiment in terms of the dependence of the transition temperature on the nanotube diameter by simulating the realistic phase-change process without artificial pressure treatments. Unlike the earlier MD calculations of the transition,[2] the model includes the carbon−carbon interaction dynamics based on a potential function that have been shown to exhibit the phonon density of states of carbon nanotubes with a sufficient accuracy.[8−10]

2. Molecular Dynamics Simulations

Water molecules were expressed by SPC/E potential.[11] SPC/E potential is expressed as the superposition of Lennard-Jones function of oxygen−oxygen interaction and the electrostatic potential by charges on oxygen and hydrogen as follows:

$$\phi_{12} = 4\epsilon_{OO}\left[\left(\frac{\sigma_{oo}}{R_{12}}\right)^{12} - \left(\frac{\sigma_{oo}}{R_{12}}\right)^{6}\right] + \sum_i \sum_j \frac{q_i q_j e^2}{4\pi\epsilon_0 r_{ij}} \qquad (1)$$

where R_{12} represents the distance of oxygen atoms and σ_{oo} and ϵ_{oo} are Lennard-Jones parameters. The Coulombic interaction is the sum of nine pairs of point charges. The SPC/E potential is known to predict the correct phase-change temperature and is widely used in micro/nano heat transfer.[12] The potential function between water molecules and carbon atoms was represented by Lennard-Jones function of the distance between the oxygen in the water molecule and the carbon atom. The parameters for the Lennard-Jones potential were $\epsilon_{oc} = 0.3126$ kJ/mol and $\sigma_{oc} = 3.19$ Å. Here, we ignored the quadropole interactions since they were found to have minute impact.[13]

The carbon interactions were expressed by the Brenner potential function[14] in a simplified form,[15] where the total potential energy of the system is modeled as

$$E = \sum_i \sum_{j(i<j)} [V_R(r_{ij}) - B^*_{ij} V_A(r_{ij})] \qquad (2)$$

Here, $V_R(r)$ and $V_A(r)$ are repulsive and attractive force terms,

* To whom correspondence should be addressed. Telephone: +81-3-5841-6421. Fax: +81-3-5800-6983. E-mail: maruyama@photon.t.u-tokyo.ac.jp.
† The University of Tokyo.
‡ E-mail: shiomi@photon.t.u-tokyo.ac.jp.
§ Kangawa University.
|| E-mail: kimura@kanagawa-u.ac.jp.

10.1021/jp071508s CCC: $37.00
Published on Web 08/02/2007

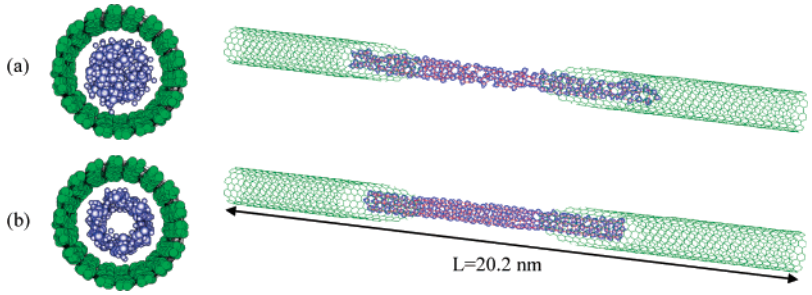

Figure 1. (a) Typical initial condition of a saturated water cluster in a (9, 9) SWNT and (b) the ice-nanotube crystallized by cooling the SWNT to 200 K ($n = 6$).

which take the Morse type form with a certain cutoff function. B_{ij}^{*} represents the effect of the bonding condition of the atoms. As for the potential parameters, we employ the set that was shown to reproduce the force constant better (Table 2 in ref 14). It has been shown that the formulation of potential function exhibits phonon dispersion with sufficient accuracy.[8−10] The inclusion of the lattice vibrations of carbon nanotubes enables us to incorporate the realistic heat transport from an SWNT to the water cluster. The thermal boundary conductance between the SWNT and the confined liquid water was previously computed to be typically about 5 MW/(m^2 K).[16]

A typical simulation begins with an initial condition with liquid water locally confined in an SWNT. Figure 1a shows the picture of a water cluster of 192 molecules adsorbed inside a (9, 9) SWNT at room temperature. The system was subjected to a periodic boundary condition in the axial direction. The cast SWNT ($L = 20.2$ nm) is longer than the sum of the cutoff distance of the Coulombic potential and the length of the water cluster, and, hence, there is no intercluster interaction through the periodic boundary. The cutoff distance of the Coulombic potential was set to be 10 nm, except for the case of (8, 8) SWNT, where the water-cluster length exceeds half the nanotube length. In the case of (8, 8) SWNT, to avoid the intercluster interaction, the cutoff distance of the Coulombic potential was reduced to 5 nm. For this case, we have also performed a simulation for cutoff distance of 2.5 nm and confirmed that the phase transition characteristics exhibit negligible dependence on the cutoff distance in the current range. The velocity Verlet method was adopted to integrate the equation of motion with the time step of 0.5 fs. We allow the center of mass of the water cluster to move along the tube axis during the simulation. After initially equilibrating the system at around 300 K, the temperature of the system was gradually decreased by applying isotropic constant heat flux to the SWNT. With negative heat flux q, heat was subtracted as

$$\mathbf{v}_i = \mathbf{v}_i \sqrt{1 + q/E_k} \tag{3}$$

where E_k is the total kinetic energy of the SWNT and $\mathbf{v}_i$ is the velocity vector of ith carbon atom. Figure 2 shows time histories of the resulting temperature of a (9, 9) SWNT and the confined water cluster for various values of q. Once the crystal is formed, a melting numerical experiment was performed with positive q in eq 3 to examine the hysteresis of the transition. Only for the case of (10, 10), in addition to the constant heat flux simulations, cooling/heating simulations were performed with a constant temperature rate.

As the casts to produce ice-nanotubes, we use armchair SWNTs with chiral-index pairs of (7, 7), (8, 8), (9, 9), and (10, 10) with diameters of $d = 0.97$, 1.11, 1.25, and 1.39 nm, which correspond to I-NTs with $n = 4$, 5, 6, and 8, respectively. To fill in the absence of an I-NT with $n = 7$, an additional case

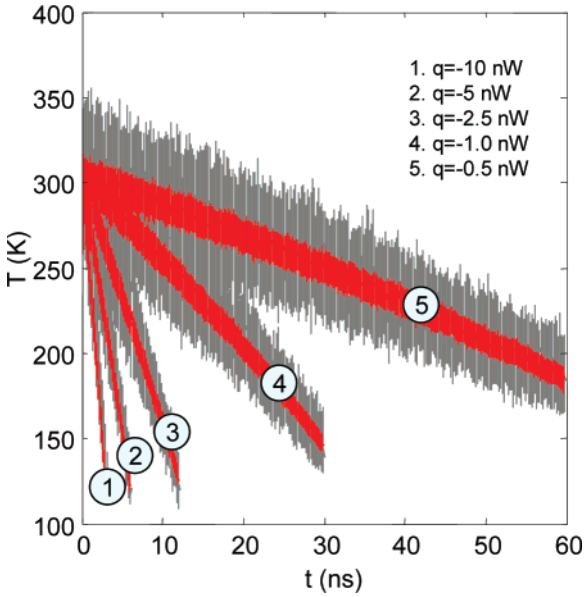

Figure 2. Typical time histories of spatially averaged temperatures of an SWNT (solid line) and the confined water cluster (dotted line) for various values of the heat flux q.

was carried out for (10, 9) SWNT ($d = 1.32$ nm). A cluster consists of 192 water molecules except for (7, 7) SWNT, where the number of water molecules was reduced to 96 due to the enhanced computational cost attributed to the relatively long elongation of the cluster in liquid phase. Although simulations were performed for values of d smaller than 0.96 nm, we did not observe formation of ice-nanotubes with $n \leq 3$ in the temperature range $T \geq 100$ K.

3. Results and Discussions

The crystallization of water can be directly monitored in the radial distribution function of water molecules. Figure 3a exhibits radial distribution functions of oxygen atoms $g_{oo}(r)$ averaged over certain time durations in the case of $n = 6$. Radial distribution functions are shown for water at (I) pretransition, (II) transition, and (III) posttransition stages to demonstrate the crystallization process on cooling the SWNT with $q = -1$ nW. The appearance of the local peaks corresponds to the interatomic length of the crystal. In addition to the equidistant peaks originated from the axial alignment of the oxygen atoms, there are distinct non-equidistant peaks below $r = 10$ Å due to the circumferential structure of the ice-nanotube; i.e., peaks correspond to nonlateral distances between oxygen atoms. By performing Fourier transform, we obtain the structural index $S(k)$, which allows us to carry out a direct comparison with the X-ray diffraction experiments.[5,6] The spectra $S(k)$ computed from $g_{oo}(r)$ profiles in Figure 3a are shown in Figure 3b. The peak

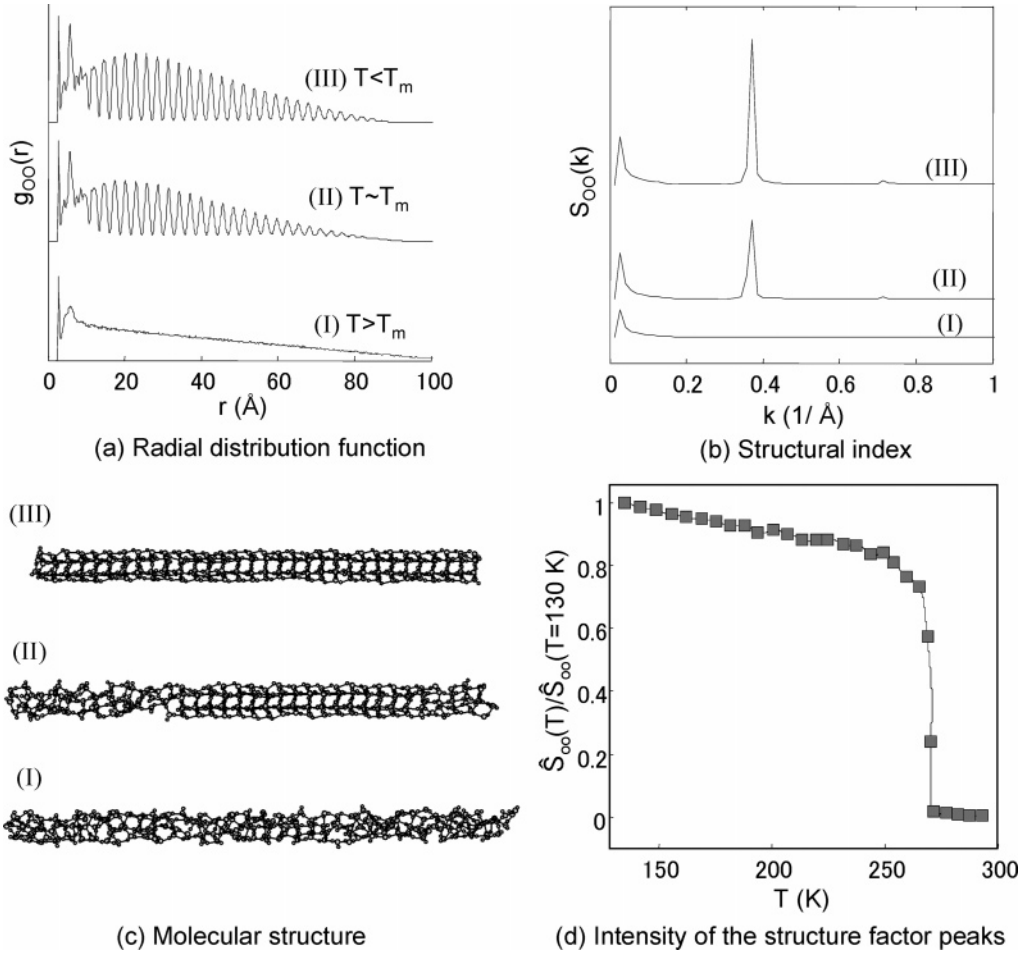

Figure 3. (a) Radial distribution functions of oxygen atoms of a water cluster confined in a (9, 9) SWNT at different stages of crystallization; (I) $T > T_m$, (II) $T \sim T_m$, and (III) $T < T_m$. (b) Corresponding structure factor $S(k)$. (c) Visual images of the molecular structures. (d) Intensity of $S(k)$ (normalized with $S(k)$ at $T = 130$ K) at different temperatures.

corresponding to the axial bond length of the ice-nanotube, though not shown here for brevity, shifts slightly depending on n, reflecting the structural variation of I-NTs. The peak position appears at around $k = 0.37$ Å^{-1} about 5% larger than 0.35 Å^{-1}, the value reported for the experiments.[5,6] The peak intensity of $S(k)$ indicates the ordering process of the I-NT as shown in Figure 3c. The pictures visualize the transition process where the crystal locally nucleates and grows in time. Figure 3d shows the time history of the peak intensity $\hat{S}_{oo}(k)$ computed by integrating the local spectrum $S(k)$ around the peak at $k = 0.37$ Å^{-1}, which is originated from the lattice distance of oxygen atoms in the axial direction. The intensity nearly saturates after the completion of the crystallization, though it grows slightly even below the freezing temperature due to the reduction of the thermal lattice vibration.

The liquid−solid phase transition can also be detected by monitoring the potential energy profiles.[3,4] The calculation of the scalar instantaneous potential energy is simpler and takes much smaller memory compared with the above-mentioned calculation of the structural factor with sufficient resolution in wave number. Parts a−c of Figure 4 show the potential energy per water molecules computed from (a) the water−water intrinsic potential (V_{ww}), (b) water−carbon interfacial interaction potential (V_{wc}), and (c) the total potential energy ($V_t = V_{ww} + V_{wc}$). In all the figures, the phase change can be detected in the jump $\Delta V = V_{liquid}(T_m + \Delta T_m/2) - V_{solid}(T_m - \Delta T_m/2)$, where T_m is the transition (melting) temperature and ΔT_m is the extent of hysteresis. Here, $T_m - \Delta T_m/2$ and $T_m + \Delta T_m/2$ are the temperatures at which the freezing and melting transitions are completed in the cooling and heating numerical experiments, respectively. Comparison of magnitudes of ΔV_{ww} and ΔV_{wc} indicates that most of the potential-energy gain due to the phase change is attributed to that of the water−water interaction. Note that the magnitude of the interaction potential energy of the water and the hydrophobic SWNT (V_{wc}) is 1 order of magnitude smaller than that of the intrinsic water−water interaction (V_{ww}).

In Figure 4a−c, for each value of d, two lines of cooling and heating numerical experiments are drawn and marked with arrows to highlight the extent of the hysteresis, ΔT_m. In the MD simulations, the restriction on the computational time limits the magnitude of heat flux $|q|$ to be much larger than reality. Therefore, the water cluster can be easily undercooled in the cooling process due to the comparable time scales between the cooling of the system and the crystal growth of the ice-nanotube, and vice versa for the heating process. For a certain value of n, ΔT_m decreases with $|q|$ and should eventually diminish when $|q|$ is small enough. As shown in Figure 4, with the smallest $|q|$ (=0.5 nW) in the current study, ΔT_m could be reduced to some extent, though the hysteresis could not be completely eliminated. As will be discussed later, in the case of a (10, 10) SWNT, I-NT was formed only in constant temperature rate simulations. The profiles for I-NT with $n = 8$ presented in Figure 4a−c are obtained at a temperature rate of 5 K/ns. Within the range of values of q explored in the current study, we always observed the formation of the I-NT structure except in some

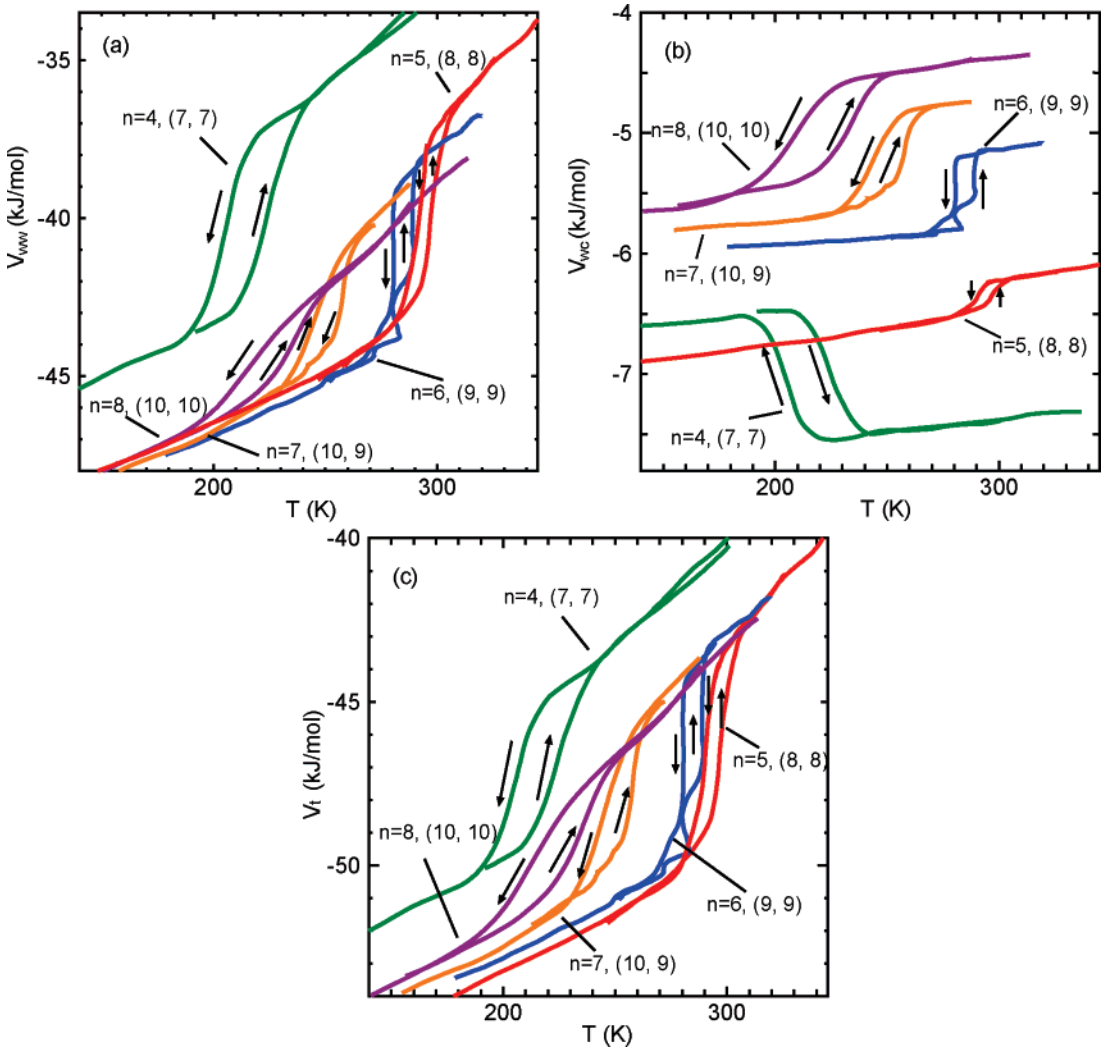

Figure 4. Temperature dependences of (a) water−water (V_{ww}), (b) water−carbon (V_{wc}), and (c) total (V_t) potential energies for various SWNT diameters (d) and numbers of ring members (n). Hysteresis is highlighted by plotting the profiles of both cooling and heating processes as denoted by arrows.

cases of (10, 10) SWNT, though glassy water is expected to form with a faster cooling rate.

The results obtained for water in (9, 9) SWNT suggests that the transition from water to I-NT is first order. Although the non-equilibrium nature of the current simulations prevents us from properly judging the order of phase transition, the profiles obtained for other cases may suggest a continuous transition, which becomes more evident as the diameter deviates from that of (9, 9) SWNT. Such a diameter dependence of order of the phase transition has been reported by Koga et al.[17]

In Figure 5, the d-dependence of T_m calculated on the basis of the above potential energy analyses is shown together with the experimental results.[6] The data are accompanied with sketches of the cross-sections of the corresponding I-NTs. We now focus on $n \geq 5$, where experimental results are available. The simulation reproduces a key quantitative feature observed in the experiments,[6] where water freezes at around room temperature in the case of $n = 5$. The agreement becomes worse for larger n, which may have to do with the increasing influence of rigidity of the SPC/E water model as the I-NT becomes unstable. The agreement is rather surprising on considering the expected size effect of the stability. Koga et al.[3] showed for rigid I-NTs ($T = 0$ K) expressed with CC (Carravetta−Clementi) and TIP4P potential models that the energy per molecule decreases by 3−6 kJ mol^{-1}, depending on n, on varying N from

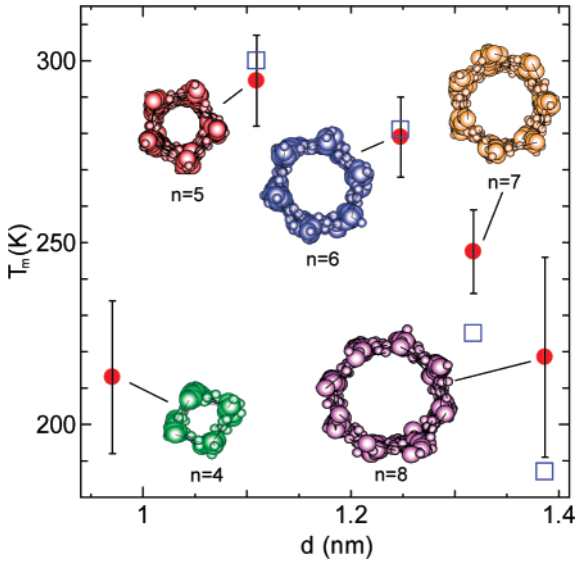

Figure 5. Transition (melting) temperature T_m for various numbers of ring members of ice-nanotubes (n). Simulation results (circles) are compared with the experimental results (squares).[6] The error bars indicate the extent of hysteresis, ΔT_m.

15 to infinity. Since the size dependence of the potential energy may influence T_m, careful investigation of the size effect would

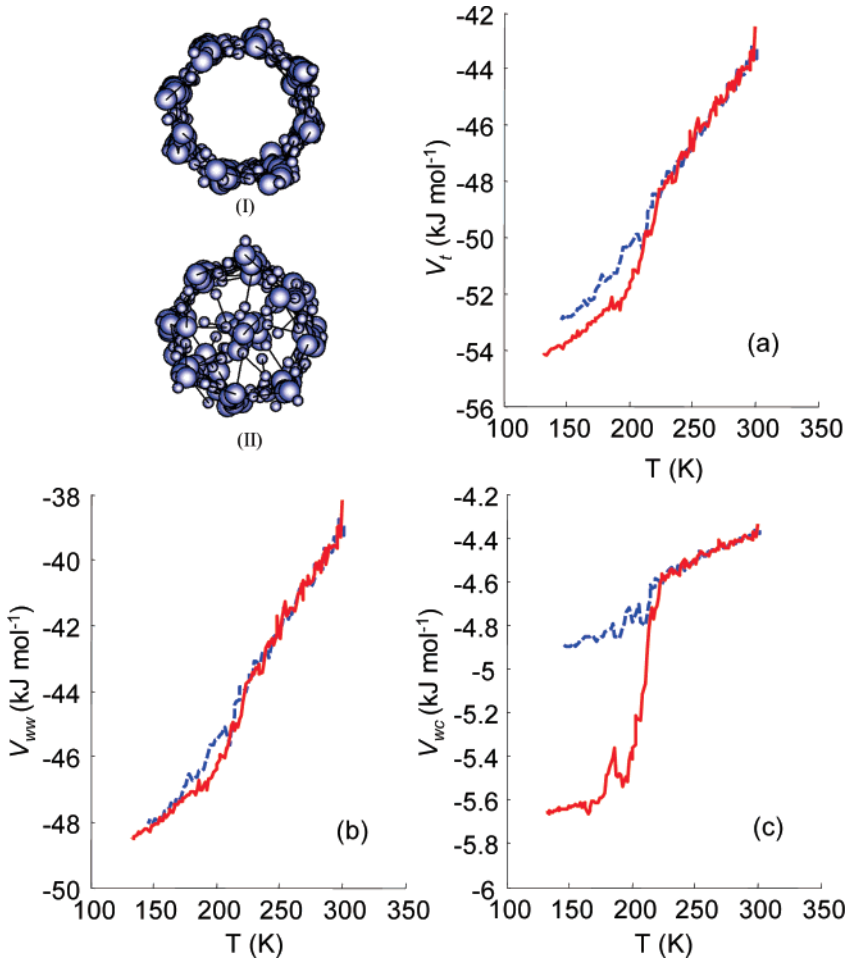

Figure 6. Stability comparison of two water-cluster structures I and II. Panels show (a) the total potential energy (V_t), (b) the contribution from water−water interactions (V_{ww}), and (c) that from water−carbon interactions (V_{wc}). Solid and dashed lines denote the profiles of structures I and II, respectively.

be necessary before concluding the quantitative agreement with the experiments. However, a thorough exploration of the size effect with the current approach including the interfacial dynamics would require considerable computational cost and therefore remains as our future task.

The simulation successfully reproduces the qualitative trend observed in the experiment;[6] i.e., T_m increases as d decreases for $n \geq 5$. As discussed in ref 6, the trend is in contrast to the capillary freezing point depression of water confined in glass microcapillaries, where T_m scales with $1/d$. In a three-dimensional capillary, T_m is determined by the balance of the volume free energy and interfacial free energy, whose dimension difference comes out as the scale $1/d$.[7] The scaling apparently does not hold when the tube is so thin that the confined water cluster consists mostly of surface. Furthermore, unlike the three-dimensional bulk ice, ice under quasi-one-dimensional confinement takes a variety of stable crystal structures depending on d, and hence the variation of the structural stability of I-NT is expected to influence the transition.[6] The current observation supports the idea, where the d-dependence of V_t in solid phase (Figure 4c) is in correlation with that of T_m (Figure 5) in $n \geq 5$. The results are consistent with the diameter dependence of lowest energy for ice-nanotubes calculated using the CC potential.[3] On the other hand, V_t of liquid water shows a minor dependence on d. It is worth pointing out that, as seen in Figure 4a, the intrinsic potential of the water−water interaction[4] does not solely explain the above correlation. It can be seen in Figure 4b that the d-dependence of the interfacial potential V_{wc} needs to be considered to achieve the correlation.

In the current simulations, an I-NT with $n = 4$ was observed, which gives rise to a maximum value of T_m at $n = 5$. I-NT with $n \leq 4$ has not been found in the experiments.[6] This could be due to the absence of SWNTs with diameters similar to the (7, 7) SWNT ($d = 0.97$ nm) in the experiment where the nanotubes of diameters from 1.09 to 1.52 nm were selectively chosen. It may also be due to the relatively unstable liquid water inside a (7, 7) SWNT. As shown in Figure 4c, the water inside a (7, 7) SWNT is less stable than the rest of the cases. This agrees with grand canonical Monte Carlo simulations,[18] where the critical d of a pore sieving effect for SPC/E water molecules adsorbed inside an SWNT was observed to lie between $d =$ 0.81 and 1.08 nm.

In the course of running numerical simulations, structure selection of the system with (10, 10) SWNT was found to be sensitive to slight changes in simulation conditions such as cooling speed and temperature control method. The I-NT formation in a (10, 10) SWNT shown in Figure 6(I) was observed only in constant-temperature rate simulations under certain simulation conditions, and the structure shown in Figure 6(II) was observed otherwise. The latter structure has been discussed in connection with the unusually volatile dynamics of the confined water.[19] By further increasing the diameter, we expect to see formation of more complicated structures such as multiwalled I-NT and ice helixes.[20] On monitoring V_t during the formations of the two ice structures in (10, 10) SWNT (Figure 6a), I-NT(I) was found to be more stable than the other ice structure (II). The energetic properties (V_{ww} and V_{wc}) show that most of the stability difference is attributed to V_{wc}, the

interfacial potential energy. The above observation of sensitivity on the simulation condition may suggest that the stability difference is counteracted by the relatively large entropy of structure II, and consequently the free energies of the two structures become similar.

4. Conclusions

The phase transition of a water cluster confined in an SWNT to an ice-nanotube was investigated using a classical molecular dynamics method. By performing non-equilibrium simulations with constant heat flux, the phase transition was identified by monitoring the structure factor and potential energies. Simulations were performed for various numbers of ring members n (4−8), and the transition (melting) temperature exhibited a maximum value at $n = 5$. For $n = 5$, T_m was confirmed to reach as high as around room temperature. For $n \geq 5$, the melting temperature obtained from the simulations agrees well with that of the experiments, not only qualitatively but also quantitatively despite the difference in the size of the system. The simulation confirms the limit of the ice-nanotube formation to be (10, 10) SWNT, beyond which ice forms a tube with the core filled with a chain of water molecules. The potential energy contribution to the phase change is generally dominated by that of water−water interactions. However, interfacial water−carbon potential energy plays a significant role in determining the dependence of T_m on d (n) and the relative stability of the tubal and nontubal ice structures in (10, 10) SWNT, where the two structures exhibit similar intrinsic stability.

Acknowledgment. This work is supported in part by the Japan Society for the Promotion of Science for Young Scientists, Grant No. 1610109, and Grants-in-Aid for Scientific Research, Grant No. 17656072.

References and Notes

(1) Sansom, S. M. P.; Biggin, P. C. *Nature* **2001**, *414*, 156.
(2) Koga, K.; Gao, G. T.; Tanaka, H.; Zeng, X. C. *Nature* **2001**, *412*, 802.
(3) Koga, K.; Parra, R. D.; Tanaka, H.; Zeng, X. C. *J. Chem. Phys.* **2000**, *113*, 5037.
(4) Byl, O.; Liu, J.-C.; Wang, Y.; Yim, W.-L.; Johnson, J. K.; Yates, J. T., Jr. *J. Am. Chem. Soc.* **2006**, *128*, 12090.
(5) Maniwa, Y.; Kataura, H.; Abe, M.; Suzuki, S.; Achiba, Y.; Kira, H.; Matsuda, K. *J. Phys. Soc. Jpn.* **2002**, *71*, 2863.
(6) Maniwa, Y.; Kataura, H.; Abe, M.; Udaka, A.; Suzuki, S.; Achiba, Y.; Kira, H.; Matsuda, K.; Kadowaki, H.; Okabe, Y. *Chem. Phys. Lett.* **2005**, *401*, 534.
(7) Jackson, K. A.; Chalmers, B. *J. Appl. Phys*. **1958**, *29*, 1178.
(8) Maruyama, S. *Physica B* **2002**, *323*, 193.
(9) Maruyama, S. *Microscale Thermophys. Eng.* **2003**, *7*, 41.
(10) Shiomi, J.; Maruyama, S. *Phys. Rev. B* **2006**, *73*, 205420.
(11) Berendsen, H. J. C.; Grigera, J. R.; Straatsma, T. P. *J. Phys. Chem*. **1987**, *91*, 6269.
(12) Maruyama, S. *Handbook of Numerical Heat Transfer*, 2nd ed.; Wiley: New York, 2006; p 659.
(13) Walther, J. H.; Jaffe, R.; Halicioglu, T.; Koumoutsakos, P. *J. Phys. Chem. B* **2001**, *105*, 9980.
(14) Brenner, D. W. *Phys. Rev. B* **1990**, *42*, 9458.
(15) Yamaguchi, Y.; Maruyama, S. *Chem. Phys. Lett.* **1998**, *286*, 336.
(16) Maruyama, S.; Taniguchi, Y.; Igarashi, Y.; Shiomi, J. *J. Therm. Sci. Tech*. **2006**, *1*, 138.
(17) Koga, K.; Gao, G. T.; Tanaka, H.; Zeng, X. C. *Physica A* **2002**, *314*, 462.
(18) Striolo, A.; Chialvo, A. A.; Gubbins, K. E.; Cummings, P. T. *J. Chem. Phys*. **2005**, *122*, 234712.
(19) Kolesnikov, A. I.; Zanotti, J.-M.; Loong, C.-K.; Thiyagarajan, P. *Phys. Rev. Lett.* **2004**, *93*, 035503.
(20) Bai, J.; Wang, J.; Zeng, C. *Proc. Natl. Acad. Sci. U.S.A.* **2006**, *103*, 19664.